Pergamon

Planet. Space Sci., Vol. 46, No. 2/3, pp. 311–322, 1998

0032–0633/98 $19.00+0.00

PII: S0032–0633(97)00035–4

Production of Tunguska-sized bodies by Earth's tidal forces

William F. Bottke Jr,[1] Derek C. Richardson[2] and Stanley G. Love[3]

[1]Division of Geological and Planetary Sciences, California Institute of Technology (Caltech), Mail Code 150-21, Pasadena, CA 91125, U.S.A.
[2]Department of Astronomy, University of Washington, Box 351580, Seattle, WA 98195-1580, U.S.A.
[3]Division of Geological & Planetary Sciences, California Institute of Technology (Caltech), Mail Code 252-21, Pasadena, CA 91125, U.S.A.

Received 30 September 1996; accepted 31 January 1997

Abstract. Tidal disruption of rubble-pile bodies (stony or icy aggregates held together by self-gravity) during close Earth encounters may produce significant numbers of Tunguska-sized (50 m) fragments. Using an *N*-body simulation to model encounters between strengthless, elongated, rotating, particulate bodies and the Earth, two disruption categories were found which produce small bodies: (a) "Shoemaker–Levy-9 type" catastrophic disruptions, where the progenitor is pulled into a line of similarly sized bodies, and (b) rotational disruptions, where the progenitor is distorted and spun-up by tidal torque such that particles are ejected along the equator. These events occur frequently at low encounter velocities (i.e. low e and i); it is predicted that Earth's tidal forces should be effective at disrupting larger bodies into Tunguska-sized fragments in this region of phase space. By creating a map of tidal disruption outcomes for the progenitor's encounter parameters and integrating over all possible values of those parameters, it is found that the tidal production rate of Tunguska-sized bodies (upper limit) was comparable with the main-belt injection rate of Tunguska-sized bodies into resonant orbits. It is concluded that tidal disruption plays an important role in maintaining the steady-state fraction of small Earth-crossing asteroids.

1. Introduction

In 1908, a small ~50 m body, possibly a carbonaceous chondrite, catastrophically disrupted 5–8 km above the Siberian wilderness in a remote area named Tunguska. The blast, equivalent to a 15–20 Mton hydrogen bomb, flattened trees over a 2000 km^2 area, roughly the size of New York City. Though scientists are still struggling today to understand the details of this event, it is clear that small bodies have the potential to produce significant damage to localized regions of our planet.

It is estimated that ~10^6 Tunguska-sized (and larger) asteroids are present in the Earth-crossing asteroid (ECA) population (Morrison, 1992). Combining this value with the mean lifetime of ECAs against Earth impact (~100 Myr; Bottke *et al.*, 1994a,b), we find the interval between Tunguska-sized impacts on Earth, on average, is 100 yr. Since humans reside on a very small fraction of the Earth's surface, the danger of dying from the blast effects of a Tunguska-type impact is minimal. On the other hand, since many humans live near coastlines, the danger of dying from an impact-generated tsunami may be more significant (Hills, 1994). For this reason, the sources of Tunguska-sized impactors need to be better characterized.

Most Tunguska-sized ECAs are thought to originate in collisions between main-belt asteroids which deliver fragments to either the 3:1 mean-motion resonance with Jupiter or the ν_6 secular resonance. It is estimated that these collisions inject one Tunguska-sized body (TSB) per year into resonant orbits (Menichella *et al.*, 1996). Once there, these bodies undergo orbital evolution which can transport them to the terrestrial planet region via chaotic increases to their eccentricity. The time for these objects to become Earth-crossing is ~1 Myr (Wisdom, 1983; Morbidelli and Moons, 1995). Those objects that have their eccentricity increased until they become Sun-grazing ($e \sim 1.0$) are defined as the "fast-track" population; those removed from resonance by perturbations from the terrestrial planets are defined as the "slow-track" population (Farinella *et al.*, 1994; Froeschlé *et al.*, 1995). Most Earth-crossing asteroids are on the "slow-track". The dynamical lifetime of ECAs against planetary collision, catastrophic collision with another asteroid, or ejection by Jupiter perturbations is on the order of 10 Myr (Milani *et al.*, 1989; Michel *et al.*, 1996).

Correspondence to: W. F. Bottke Jr

Using the injection rate of TSBs into resonance (one object per year) and the collision rate of TSBs on Earth (one object per 100 yr), Menichella *et al.* (1996) estimate that 1% of all TSBs on resonant orbits impact the Earth. To maintain a steady-state population of 10^6 TSBs, less than 10% of all the TSBs entering resonant orbits become part of the ECA population. This paradigm, however, may neglect an important source mechanism for TSBs in the ECA region. Weak ECAs should be vulnerable to disruption by tidal forces during close encounters with the Earth and other terrestrial planets. Because close planetary encounters occur more frequently than collisions, asteroidal tidal disruption may be capable of producing numerous small bodies, possibly even enhancing the population of TSBs near Earth.

To investigate the role of tidal disruption in producing TSBs, our paper uses the following format. We first review previous work on tidal disruption and the evidence that many asteroids approaching the Earth are weak (Section 2). Next, we describe a numerical model capable of simulating the tidal disruption of weak particulate asteroids encountering the Earth (Section 3). By analyzing the outcome statistics from asteroid encounters we gauge the effectiveness of disruption over a variety of encounter parameters (Section 4). Finally, we predict the relative efficiency of TSB production via tidal disruption (Section 5) and examine the observed population of Earth-crossing asteroids for evidence of tidal forces at work (Section 6).

2. Tidal disruption and rubble-pile asteroids

Tidal disruption was first investigated by Roche (1847) (see Chandrasekhar, 1969), who derived the distance (now called the Roche limit or Roche radius) at which a self-gravitating non-rotating liquid satellite on a circular orbit around a rigid spherical planet can no longer maintain an equilibrium figure:

$$R_{\text{roche}} = 1.51\left(\frac{M_{\text{pl}}}{\rho_{\text{sat}}}\right)^{1/3} = 2.45 R_{\text{pl}}\left(\frac{\rho_{\text{pl}}}{\rho_{\text{sat}}}\right)^{1/3} \quad (1)$$

where M_{pl}, R_{pl}, and ρ_{pl} are the mass, radius, and density, respectively, of the planet and ρ_{sat} is the density of the satellite. Equation (1) shows that tidal forces are so weak that even objects with zero tensile strength need close encounters to disrupt. For example, a body with a density of $2\,\text{g cm}^{-3}$ disrupts if it orbits the Earth at a distance less than $3.4R_{\oplus}$ where $R_{\oplus}$ is the Earth's radius. The disruption limit for a body approaching a planet on a parabolic orbit is even smaller (Sridhar and Tremaine, 1992; Asphaug and Benz, 1996):

$$R_{\text{disrupt}} = 0.69 R_{\text{roche}}. \quad (2)$$

Thus, an object with a density of $2\,\text{g cm}^{-3}$ would only disrupt after passing within $2.4R_{\oplus}$ of the Earth. Since conventional wisdom (until recently) held that comets and asteroids had tensile strength and/or internal dissipation, many early studies reported that small bodies either cannot tidally disrupt, or disrupt only under special circumstances (Jeffreys, 1947; Öpik, 1950; Sekiguchi, 1970; Aggarwal and Oberbeck, 1974; Mizuno and Boss, 1985). Related work by Dobrovolskis (1982, 1990) set strict limits on the size, strength, and material properties required to produce tidal disruption.

In the 1990s, sophisticated numerical and analytical studies investigated tidal disruption of spherical non-rotating strengthless objects (Boss *et al.*, 1991; Sridhar and Tremaine, 1992; Asphaug and Benz, 1996; Solem and Hills, 1996). A good review of the issues involved and techniques used can be found in Asphaug and Benz (1996). These models reported that tidal disruption can occur among comets and asteroids if they are "rubble-piles", aggregates of strong component material held together by self-gravity rather than tensile strength. A growing body of evidence suggests such objects may be common:

- Öpik (1966) suggested comet Ikeya Seki had a rubble-pile structure after observing it disrupt during a close encounter with the Sun. More recently, Asphaug and Benz (1994, 1996) concluded that comet Shoemaker–Levy-9 (SL9) could only have disrupted into 20 or so similar-sized fragments during a close encounter with Jupiter if the progenitor had been virtually strengthless.
- Harris (1996) showed that none of the 107 asteroids smaller than 10 km with known rotation periods rotate faster than the theoretical break-up limit for a strengthless, gravitating object. This result implies that rubble-pile composition may be common, since solid objects could theoretically rotate at nearly any speed.
- Large craters have been found on small bodies such as Ida, Gaspra, and Phobos. These craters, such as Stickney on Phobos, are formed in the "gravity scaling" regime, where the ultimate size of the crater is controlled by the target's self-gravity rather than its physical strength. Craters formed in the gravity regime require a weak or fragmented target, which can exist prior to impact or can be produced by the crater-forming impact itself (i.e. crater excavation is preceded by an advancing shock front, which shatters the material as it passes through). The size of the projectile needed to form the large crater Stickney on Phobos in the strength regime would instead disrupt Phobos (Asphaug and Melosh, 1993). Numerical hydrocode simulations of asteroid collisions suggest that small to moderately sized projectiles striking an undamaged asteroid produce highly fractured target bodies, even though larger blocks of material can remain intact (Greenberg *et al.*, 1994, 1996; Love and Ahrens, 1996).
- Bottke and Melosh (1996a,b) showed that rapidly rotating rubble pile asteroids encountering the Earth could be split into multiple co-orbiting components by tidal forces. By showing that this mechanism could produce binary asteroids, they were able to reproduce the observed fraction of doublet craters on the Earth, Venus, and Mars if most ECAs are rubble-piles.

Thus, tidal disruption of rubble-pile ECAs, if common, could provide a source for a substantial fraction of the small bodies which impact the Earth.

3. Numerical model

In order to characterize the mass loss produced by tidal disruption near the Earth, we use the numerical techniques

described by Richardson (1993, 1994, 1995) to model close Earth flybys of aggregates of spherical particles held together solely by their own self-gravity (i.e. a rubble-pile). A fourth-order polynomial predictor–evaluator–corrector integration engine was used to advance the particle positions and velocities forward in time. To increase precision, the calculation was performed in the progenitor's center-of-mass reference frame. Note that additional details and results will be provided in Richardson *et al.* (1997).

Our model is similar to those used in the past by Asphaug and Benz (1996), Solem and Hills (1996), and others. In fact, if we were to use the same non-rotating spherical progenitor that they do, we would obtain nearly identical results. Our runs, however, introduce several new features which allow us to more realistically treat encounters between rubble-pile progenitors and the Earth.

First, we give our progenitor an elongated shape which closely mimics the shapes of real Earth-crossing asteroids (McFadden *et al.*, 1989; Ostro, 1993; Ostro *et al.*, 1995a,b). Our progenitor, composed of 247 spherical particles, was given dimensions of $2.8 \times 1.7 \times 1.5$ km ($1.8 \times 1.1 \times 1.0$ normalized), somewhat similar to the shape of Earth-crossing asteroid 4769 Castalia (Hudson and Ostro, 1995a). Other groups have so far only investigated spherical progenitors, which are intrinsically more stable against tidal disruption than other rubble-pile configurations (i.e. spheres have a lower potential energy). Use of an elongated progenitor, however, complicates our test runs, since we must keep track of the rotation phase (orientation of the progenitor's long axis) at perigee. We define this rotational phase using the angle θ; when $\theta = 0^\circ$, the long axis or its projection in the orbit plane points directly towards the Earth.

Second, we allow our progenitor to rotate, treating spin periods of $P = 4$, 6, 8, 10, and 12 h. Previous models have used progenitors without spin, since (a) objects have a nearly equal probability of encountering the Earth with a prograde or retrograde spin, making the zero spin case a reasonable representative case, and (b) it is simpler. This "average" progenitor ($P = \infty$), however, does not necessarily produce the median break-up outcome. Our results indicate that the median break-up outcome is instead dominated by objects with prograde spins, which happen to be very susceptible to tidal disruption. To account for rotation, we need to define the orientation of the progenitor's spin axis at perigee. We do so using two angles: α, the angle between the rotation pole and the normal of the progenitor's orbit plane, and β, the projected angle between the pole and the vector connecting the progenitor with the center of the Earth at perigee measured in the orbital plane.

Third, we define the trajectory of the progenitor near Earth as a hyperbola using two parameters: the progenitor's encounter velocity at "infinity" (v_∞, defined as the velocity of a body before the gravitational acceleration of Earth becomes significant) and its perigee distance (q). Previous models often simulated encounters between small bodies and a planet using a parabolic path. These trajectories can provide a useful approximation, but they are not as realistic as hyperbolic trajectories for most comets and asteroids near the Earth. The parameters q and v_∞, in conjunction with the rotation period of the progenitor (P), will play a critical role in determining whether a given encounter produces a tidal disruption.

Fourth, we include friction or energy dissipation between the particles using a coefficient of restitution (i.e. the ratio of the rebound speed to the impact speed) defined by the variable ϵ. For the cases shown in this paper, $\epsilon = 0.8$. Our tests show tidal disruption is largely insensitive to the choice of ϵ as long as collisions are inelastic ($\epsilon < 1$).

The bulk density of the progenitor was chosen to be $2\,\mathrm{g\,cm^{-3}}$ so it would correspond to typical km-sized body densities (e.g. Phobos and Deimos were found to have densities near $2\,\mathrm{g\,cm^{-3}}$ (Thomas *et al.*, 1992); 243 Ida was estimated to have a bulk density near 2.0–3.1 $\mathrm{g\,cm^{-3}}$ (Belton *et al.*, 1995)) and porous stone. Individual particles have densities of $3.6\,\mathrm{g\,cm^{-3}}$, similar to chondritic meteorites (Wasson, 1974). We do not report on our test runs with cometary bulk densities in this paper, because we do not expect many comets to tidally disrupt near the Earth. Long period comets typically have such high encounter velocities with Earth (mean encounter velocity is $\sim 55\,\mathrm{km\,s^{-1}}$ (Weissman, 1982)) that few are expected to undergo tidal disruption. The contribution of short-period comets to the near-Earth object population is thought to be negligible (Morrison, 1992). We do not address the issue of extinct comets within the Earth-crossing asteroid population.

The starting distance of the progenitor from the planet is 15 Roche radii, large enough to ensure planetary perturbations are negligible at the outset, but small enough to make exploration of parameter space practical. Each run is terminated at a post-encounter distance where most of the dynamical activity related to tidal disruption is completed ($\sim 60\,R_\oplus$).

4. Results

We recognize two types of tidal disruption when rubble-pile asteroids encounter the Earth.

4.1. *Catastrophic or "SL9-type" disruptions (class "S")*

For very close or slow encounters, the equipotential surface of the rubble-pile asteroid is modified from a spheroid into a pencil-like shape by Earth's tidal forces. Particles outside the new equipotential surface move or roll "downhill" to fill in that shape, though friction and their own inertia prevent them from arriving at their new positions instantaneously. As the pile recedes from the planet, the equipotential surface contracts, leaving many particles distributed along the former pencil-like shape. Gravitational instabilities cause most of these particles to clump into a number of roughly equal-sized bodies that look very much like a "string of pearls" (Fig. 1, top left). This disruption type is analogous to that seen when comet SL9 was pulled apart near Jupiter (Sridhar and Tremaine, 1992; Boss, 1994; Asphaug and Benz, 1994, 1996). We classify the disruption as "S" type when the largest remaining fragment retains less than 50% of the progenitor's original mass. Numerical modeling supports the

idea that "S" class outcomes can produce crater chains on the Moon but not on the Earth (Bottke *et al.*, 1997).

4.2. *Rotational tidal disruptions (class "B", "M", "N")*

When a point mass encountering the Earth reaches perigee, the gravitational acceleration pulling the object towards Earth equals the centrifugal force trying to throw it from the Earth. For real bodies such as our elongated rubble-pile asteroid, however, this balance is lost. Instead of experiencing equal forces, the end of the asteroid nearest to Earth experiences a slight excess of gravitational force pulling it radially towards Earth, while the end of the asteroid furthest from Earth experiences a slight excess of centrifugal force pulling it radially away from Earth. This differential force results in a torque which pulls the asteroid's long axis towards the radial line stretching from the asteroid's center of mass to the Earth's center. Objects with longer moment arms at perigee (i.e. spherical bodies have uniformly small moment arms, elongated asteroids have moment arms which vary depending on their orientation at perigee) are more susceptible to tidal torque. In many cases, tidal torque may accelerate the asteroid's rotation rate and increase its length. (Variations on this theme can be found in Boss *et al.* (1991), Boss (1994), and Solem and Hills (1996).) If the torque is strong enough, the ends of the distorted asteroid may be lost into space along the asteroid's equatorial plane. Keplerian shear (wherein bodies closer to the asteroid's center of mass orbit faster than those further away) among these ejected bodies produces spiral deformations similar to those seen in models of stellar collisions (Benz and Hills, 1987; Benz *et al.*, 1989). We (arbitrarily) divide this disruption regime into two groups: "B" breakup with mass shedding of clumps and particles where between 10% and 50% of the progenitor's mass is lost (Fig. 1, top right); and "M" mild mass shedding of small fragments where less than 10% of the progenitor's mass is lost (Fig. 1, bottom left). A fourth category, "N", describes outcomes where no mass is lost but tidal torques may still reshape the asteroid or change its spin rate (Fig. 1, bottom right) (e.g. the strange shape of 1620 Geographos reported by Ostro *et al.* (1995a, 1996) may be an example of a tidally distorted body).

Figure 2 shows the results for progenitors with rotation periods of $P = 6$ h encountering the Earth over varying values of q and v_∞. "S" class events occur from $q \approx 2R_\oplus$ at 3 km s^{-1} to $q \approx 1.01R_\oplus$ for velocities near 21 km s^{-1}. Rotational tidal disruption ("B" and "M") range from $q \approx 3R_\oplus$ at 3 km s^{-1} to $q \approx 1.4R_\oplus$ at 21 km s^{-1}. In general, we find that low values of P, q and v_∞ result in more catastrophic disruptions. Our results, however, do not always follow a simple pattern (e.g. the "N" outcome for $q = 1.4R_\oplus$, $v_\infty = 21.1$ km s^{-1}). This complication is due to noise in θ, the rotation phase of the progenitor at perigee, as q and v_∞ change. Computational limitations prevented us from using the exact same value of θ for each choice of P, q, v_∞, but the overall trends in Fig. 2 are clear.

Though not shown, we have completed plots similar to Fig. 2 for progenitors having a variety of different rotation periods. We find that faster rotation periods ($P = 4$ h) enhance disruption, increasing the range of q, v_∞ values where "S", "B", and "M" disruptions occur. Slower rotation periods ($P = 8$, 10, 12 h), however, decrease this range. We expect that tests using very long periods will take us close to regimes explored using a spherical nonrotating progenitor by Asphaug and Benz (1996) and Solem and Hills (1996).

As explained previously, disruption can be assisted by tidal torque, whose effectiveness changes depending on θ, the rotational phase of the asteroid's leading long axis at perigee. For $-90° \geq \theta \geq 0°$ (i.e. when the leading long axis is rotating towards the Earth in the prograde sense), tidal torque and centrifugal force work together to enhance disruption. For $0° \geq \theta > 90°$ (i.e. when the leading long axis is rotating away from the Earth), tidal torque and centrifugal force oppose one another to deter disruption. Thus, to generate Fig. 2, we chose rotational phase angles of $-90° < \theta < 0°$ for all computed runs.

The progenitor's rotation pole orientation can also change the outcome of an encounter. Figure 2 was completed using prograde progenitors with $\alpha = 0°$. Real asteroids, however, have randomly oriented spin axes, with an equal probability of encountering the Earth with a prograde or retrograde rotation, making our results applicable only part of the time. Although computational limitations prevented us from testing α and β for each set of q, v_∞, P, and θ, we did test enough cases to determine the following trend: asteroids undergoing "S", "B", or "M" class events when $\alpha = 0°$ continue to undergo the same class of disruption so long as rotation is prograde (i.e. $\alpha \geq 90°$), though the severity of mass shedding within a class decreases as α approaches 90°. Once rotation becomes retrograde ($\alpha > 90°$), nearly all mass shedding ends.

In summary, only half of the objects encountering the Earth are likely to have their long axis orientated such that a disruption event is likely. Of the rest, only half encounter the Earth with prograde rotation (i.e. $\alpha < 90°$). Thus, we find that an elongated Earth-crossing rubble-pile asteroid has, at most, only a 25% chance of undergoing a tidal disruption event each time it encounters the Earth. These results can be used to predict how many Tunguska-sized objects can be produced from ECAs by tidal forces.

5. Production of Tunguska-sized bodies by tidal disruption

The production frequency of TSBs from tidal disruption can be estimated by combining the following components.

5.1. *Map of tidal disruption outcomes near the Earth*

Figure 2 shows the critical encounter parameters (q, v_∞) needed to produce a "S", "B", or "M" class disruption for a $P = 6$ h prograde progenitor. Similar maps have been produced for other rotation periods ($P = 4$, 8, 10, 12 h). Since it is computationally prohibitive to map disruption outcomes for all possible values of θ, α, and β while varying P, q, and v_∞, we test a more limited set and treat the remainder statistically, dividing our estimate of

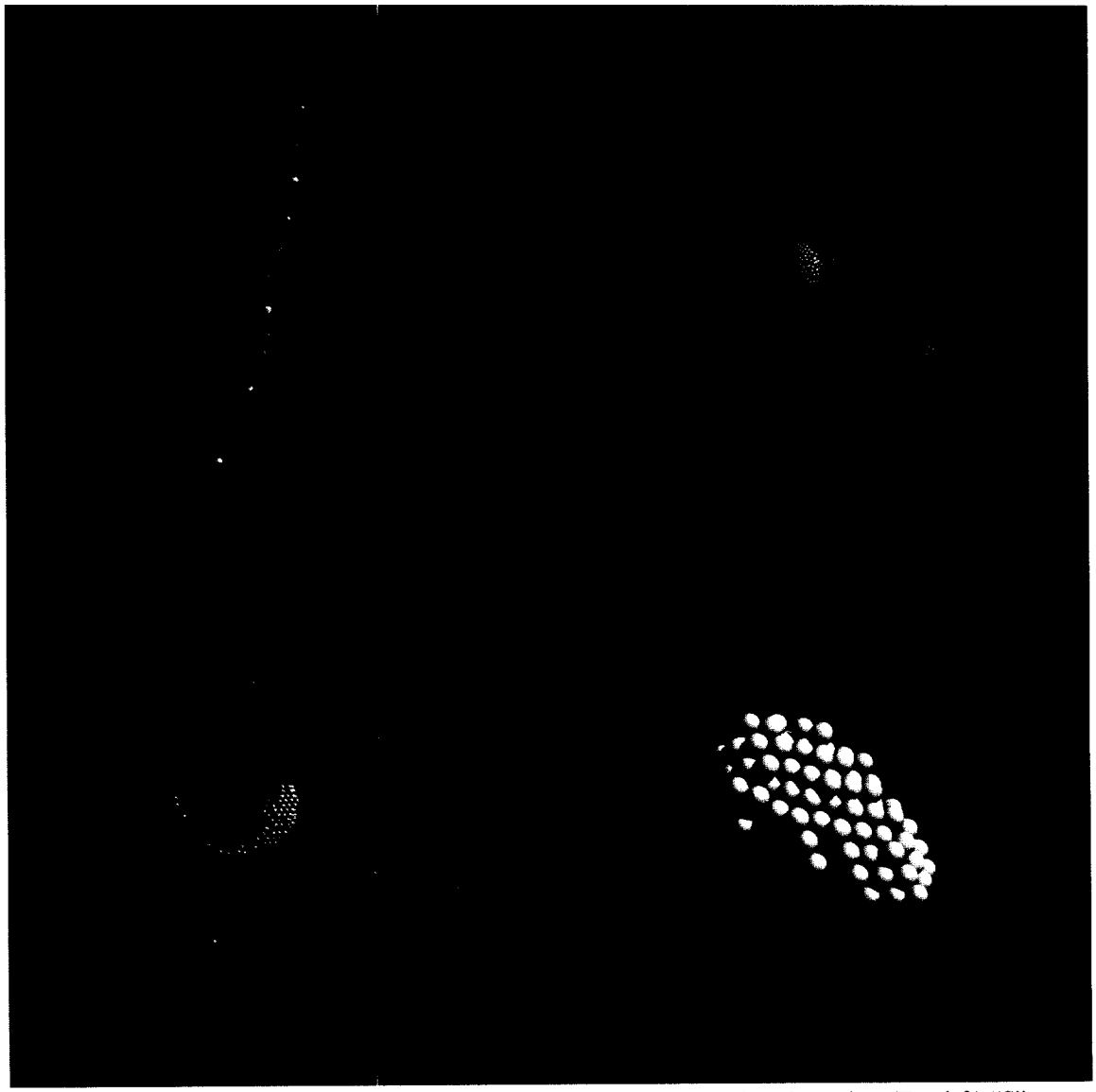

Fig. 1. Snapshots of four classes of tidal disruption. In decreasing order of severity: (Top left) "S", a "Shoemaker–Levy-9-type" catastrophic disruption where the progenitor forms into a line of roughly equal size clumps (i.e. a "string of pearls") and leaves less than 50% of its mass in the largest fragment; (Top right) "B", a break-up with mass shedding of clumps and single particles, leaving the progenitor with 50–90% of its original mass; (Bottom left) "M", mild mass shedding of clumps or particles, leaving the progenitor with over 90% of its original mass; and (Bottom right) "N", no mass loss but possible reshaping of the progenitor accompanied by spin-up or spin-down

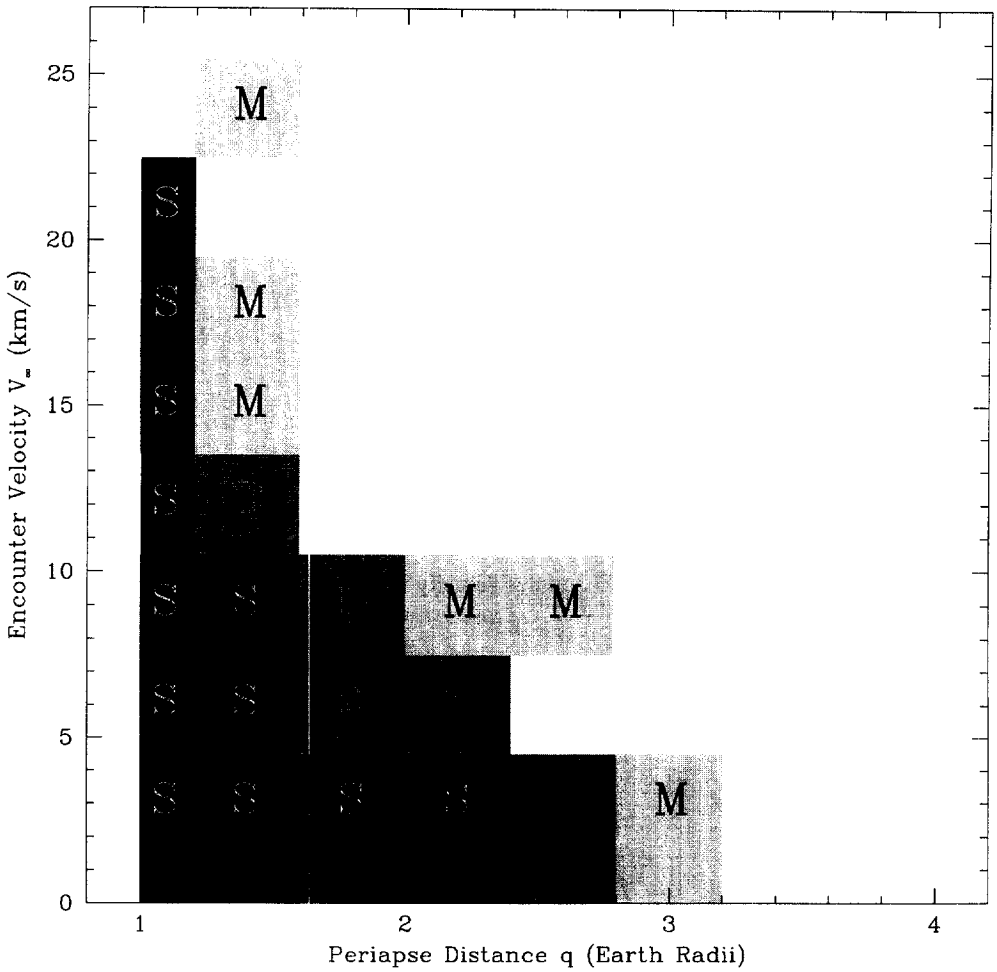

Fig. 2. Tidal disruption outcomes for rubble-pile progenitors with rotation periods of $P = 6$ h encountering the Earth for various values of q (1.01, 1.4, 1.8, 2.2, 2.6, 3.0, 3.4, 3.8$R_\oplus$) and v_∞ (3.4, 6.2, 9.1, 12.1, 15.1, 18.1, 21.1, 24.1 km s^{-1}). See Fig. 1 for key to symbols. The blank spaces of the plot are "N" class outcomes. The jitter seen in the outcomes is caused by noise in θ as q and v_∞ change

the disruption frequency by 4 based on the results presented in Section 4.

5.2. *Probability distribution of ECA encounter velocities with the Earth*

Assuming the 197 ECAs discovered as of April 1996 (from the Minor Planet Center via the database of D. Tholen) provide a representative sample of the entire ECA population, we used the technique of Bottke *et al.* (1994a,b) to calculate the probability distribution of encounter velocities with Earth (Fig. 3). The average encounter velocity ($\langle v_\infty \rangle$) for this distribution is 12.47 km s^{-1}, though many different values of v_∞ were used to generate our results.

5.3. *Probability of ECAs encountering Earth*

Using the same technique and ECA population described above, we calculated the average intrinsic encounter probability of ECAs with Earth: $\langle P_i \rangle = 1.12 \times 10^{-16}$ km^{-2} yr^{-1}. The encounter probability for a given asteroid was found by multiplying this value by q^2 (π is already included in P_i) and by the gravitational focusing factor $(1 + v_q^2/v_\infty^2)$, where v_q is the escape velocity of the Earth at a distance q from its center.

5.4. *Probability distribution of rotation periods among ECAs*

The rotation period distribution of asteroids smaller than 10 km can be approximated as a Maxwellian with a mean period of 6 h (Fig. 4) (A. Harris, personal communication). Since Harris' results (Harris, 1996) imply that no asteroid is currently in a state of tension, this distribution is truncated at 3.1 h (i.e. where our test asteroids would fly apart from centrifugal force). The distribution is also scaled for the 20% of the ECA population which are extremely slow rotators (e.g. 4179 Toutatis (Hudson and Ostro, 1995b)). For this calculation, we assume such bodies cannot tidally disrupt, though this approximation may be overly conservative (e.g. Asphaug and Benz, 1996).

5.5. *Size–frequency distribution of (rubble-pile) asteroids in the ECA population*

The ECA size–frequency distribution is shown in Fig. 5 (Morrison, 1992). This distribution was calculated using

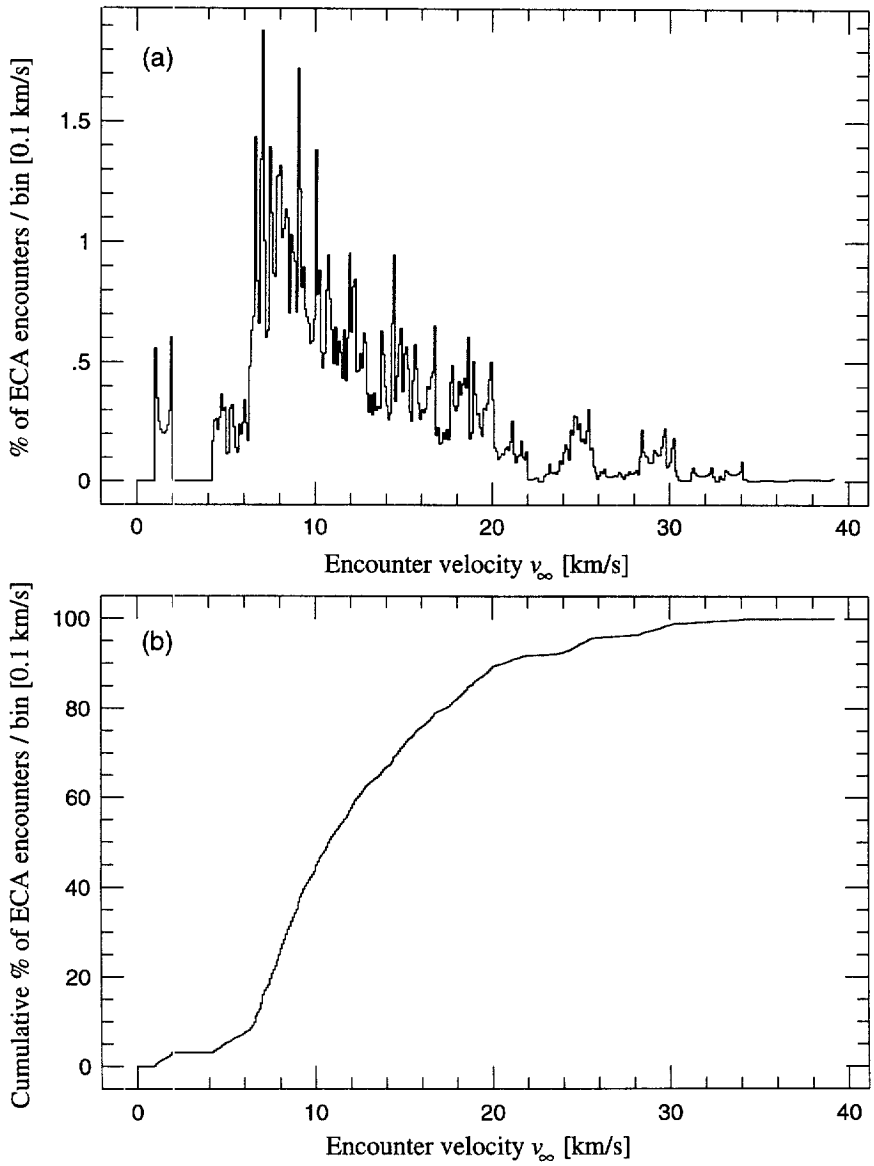

Fig. 3. (a) Probability distribution of encounter velocities at "infinity" (v_∞) with Earth by the 197 asteroids that are Earth-crossers. The mean velocity for the distribution is 12.5 km s^{-1}. The mean intrinsic collision probability is 1.12×10^{-16} km^{-2} yr^{-1}. (b) The cumulative probability distribution of encounter velocities at "infinity" (v_∞) with Earth by the same population

data taken from the lunar cratering record, the terrestrial cratering record, and microbarograph records of atmospheric explosions (G. Shoemaker, personal communication). At the right-hand side of the size distribution, we insert the three largest known ECAs (9.6 km, 11 km, 12 km). Since the cratering history of the Moon suggests the impact rate in the Earth–Moon system has been constant over the last 3 Gyr (Grieve and Shoemaker, 1994), we assume the ECA population is in a steady-state. We also assume that rubble-pile asteroids must be 250 m in diameter or larger, the limit where catastrophic disruptions are controlled by the self-gravity of the target rather than its physical strength (Love and Ahrens, 1996). Approximately 40 000 ECAs have diameters larger than 250 m, with an uncertainty factor of two.

Integrating these components, we estimate that the total mass shed by rubble-pile ECAs is nearly 6×10^{10} g yr^{-1}. This result is relatively insensitive to modifications to either end of the ECA size–frequency distribution: increasing the rubble-pile limit to 1 km only decreases the mass shedding rate by 15%, while decreasing the size of the largest ECA to 7 km decreases the rate by 25%.

We believe it is premature to predict the size–frequency distribution of material shed during a tidal disruption event, since we have only tested progenitors composed of spherical particles which are 250 m in size. Future work will examine this issue using a range of particles sizes and a greater number of small particles. Nevertheless, we can use our results to set some reasonable upper limits. If all the mass shed in tidal disruptions (6×10^{10} g yr^{-1}) were in the form of TSBs (50 m objects), their production rate would be 0.4 yr^{-1}, comparable with the injection rate of TSBs entering the 3:1 or ν_6 resonances (one object per year (Menichella *et al.*, 1996)). Since neither the size distribution of component material in a rubble-pile nor the supply rate of 50 m bodies from the resonances to the

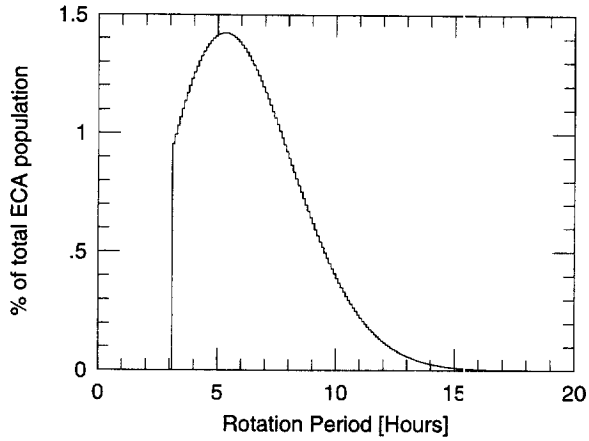

Fig. 4. The probability distribution of ECA rotation periods, estimated to be a Maxwellian with a mean period of 6 h. The distribution is truncated at 3.1 h, the limit where our rubble-pile progenitors disrupt from centrifugal force, and scaled for the 20% of the ECA population which are extremely slow rotators

"slow-track" are known, it is difficult to say which source is more important for replenishing the nearly 10^6 Tunguska-sized ECAs.

Note that the average mass shedding rate given here overlooks the episodic nature of tidal disruption events. Our results show that the lifetime of a rubble-pile against "S" class events is 450 Myr, the lifetime against a "S" or "B" class events is 260 Myr, and the lifetime against "S", "B", or "M" class events is 120 Myr. Thus, for all km-sized ECA's (2100), we find that "S"-type events occur near the Earth once every 210 000 yr, "S" and "B" events once every 120 000 yr, and "S", "B", "M" events once every 55 000 yr. The disruption of such an Earth-crossing asteroid should place multiple small bodies into orbits similar to that of the progenitor until planetary close encounters cause the objects to spread.

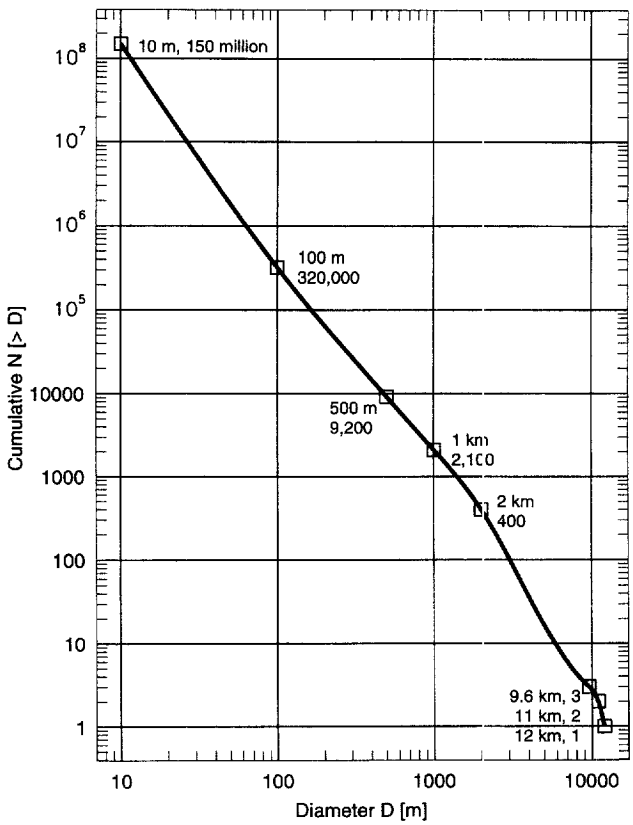

Fig. 5. Estimated number of Earth-crossing asteroids larger than a given diameter (based on Morrison (1992)). The uncertainty in the distribution is a factor of 2

6. Evidence for tidal disruption among ECAs

Since bodies encountering Earth with low v_∞ orbits are more likely to undergo tidal disruption, an examination of this region of phase space should show a greater abundance of tidal ejecta and tidally disrupted/distorted bodies. To map these low v_∞ regions, we calculated mean v_∞ values between test bodies spaced at regular intervals in (a, e, i) space and the Earth using the technique of Bottke *et al.* (1994a,b) (i.e. the test bodies have semimajor axes a between 0.05 and 4.0 AU, separated by $\Delta a = 0.05$ AU; eccentricity e between 0.0 and 0.99, separated by $\Delta e = 0.01$, and inclination i between 0° and 35°, separated by $\Delta i = 5°$).

Figure 6 shows two velocity contour maps produced from these results. Contours have units of km s^{-1}. Figure 6a shows that test bodies with 5° inclination have low v_∞

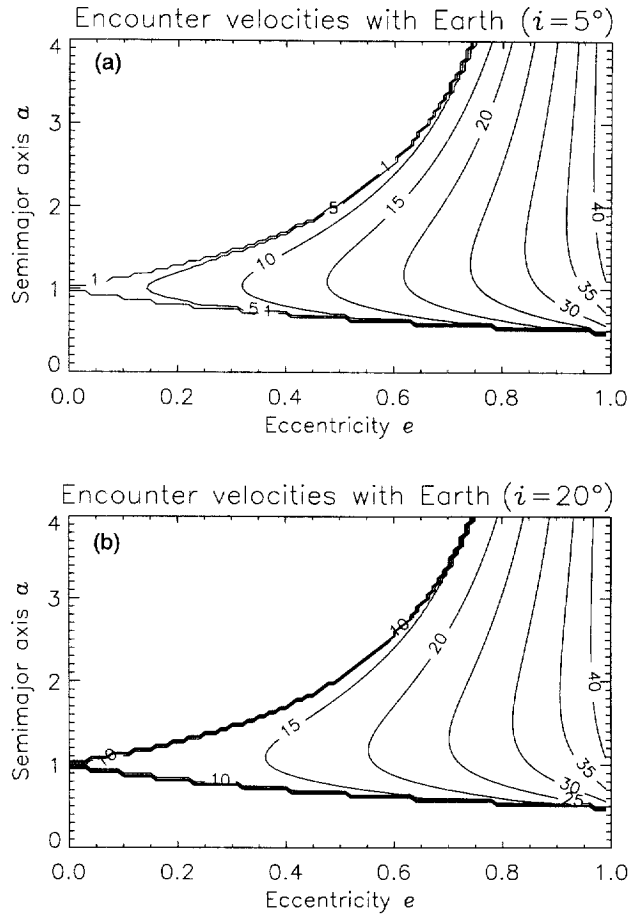

Fig. 6. Contour plots in (a, e) space of mean v_∞ values for test bodies encountering the Earth with (a) $i = 5°$, and (b) $i = 20°$. Contours have units of km s^{-1}. The lowest velocities are found where e is small and perihelion (q) and aphelion (Q) are near 1 AU

values when e is small and perigee (q) and apogee (Q) are near 1 AU. Figure 6b ($i = 20°$) shows a similar trend, though the higher inclination raises the lowest v_∞ level enough to inhibit most tidal disruptions. Since ECAs generally adhere to the same v_∞ contours as their progenitors (Bottke *et al.*, 1996c), tidal ejecta should be common in the low e, i regions of ECA space.

Low v_∞ ECAs collide with the Earth more frequently that other ECAs. They also penetrate Earth's atmosphere more deeply before exploding, such that objects smaller than 50 m may be capable of causing Tunguska event-like effects (Passey and Melosh, 1980). If a substantial fraction of small ECAs are tidal ejecta, Tunguska-type events may occur somewhat more frequently than predicted.

Tidal disruption in this region should enhance the population of Tunguska-sized ECAs and deplete the population of rubble-piles. A qualitative examination of the orbits and diameters of all known ECAs may corroborate our results. We caution, however, that the observed sample of ECAs (197) is so small that it is unlikely to be representative of either the km-sized ECAs (2100) or the 50 m ECAs ($\sim 10^6$) (Morrison, 1992); at best, the ECA population is only complete to absolute magnitude $H = 13.5$, corresponding to a 6 km "S" class asteroid or a 12 km "C" class asteroid (Rabinowitz, 1994). In addition, we know this sample is biased, since observers look for asteroids near the ecliptic and at opposition, where they can take advantage of increased brightness, increased numbers, and favorable rates of motion (Jedicke, 1996).

Figure 7 shows the orbital positions of these bodies in (a, e) space and (a, i) space. Any asteroid larger than 3 km is plotted with a large open circle, while any asteroid smaller than 200 m is plotted with a small open circle. The remaining asteroids are plotted with open circles linearly scaled between these limits. Asteroids crossing Earth's orbit lie between the $q = 1$ AU and $Q = 1$ AU lines, while asteroids crossing the orbits of the other planets lie between other (q, Q) lines. For example, asteroid 1620 Geographos ($a = 1.2455$ AU, $e = 0.3354$, $i = 13.3°$) crosses the orbit of Earth and Mars but not Mercury or Venus.

A qualitative examination of Fig. 7 reveals many small bodies at low e, i. Few large bodies with low i can be found near $q = 1$ AU, though it is not clear if tidal forces or collisions with the Earth is wholly responsible. Nevertheless, these structural features are consistent with the implications of tidal disruption results and Fig. 6.

Interestingly, it has been suggested that an "excess" number of 10–50 m ECAs may exist in the low e region

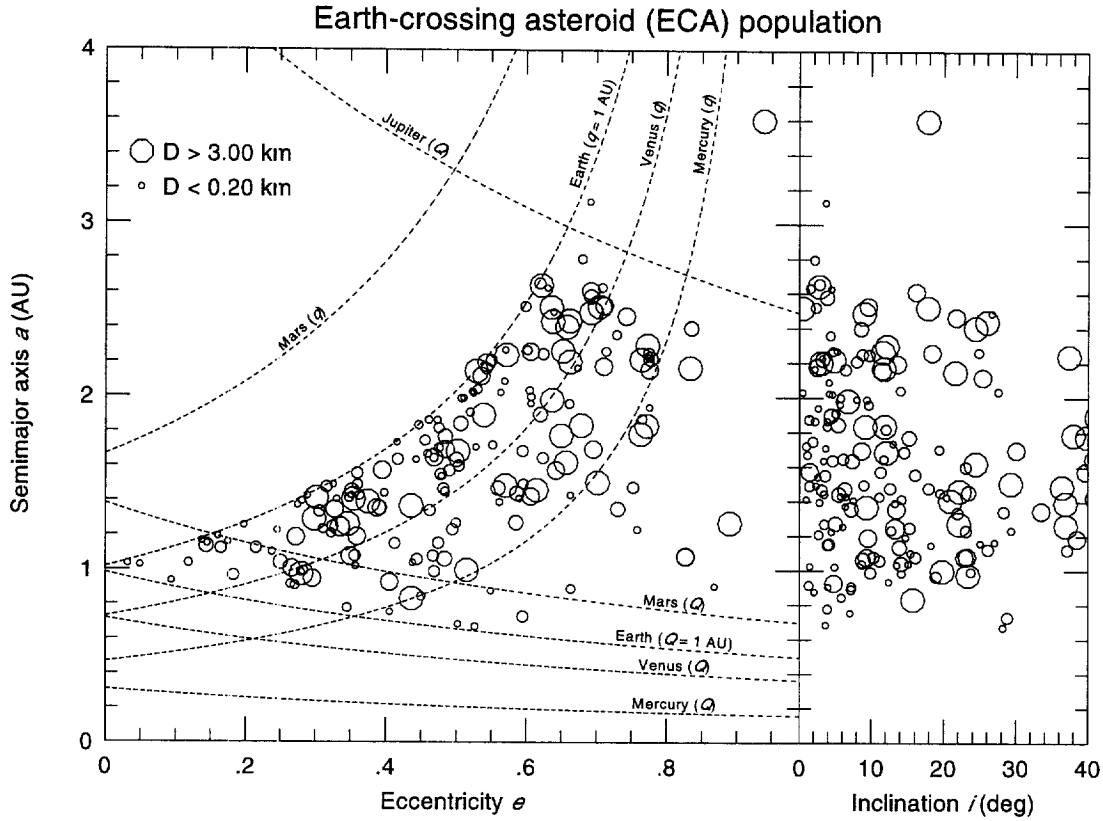

Fig. 7. Orbital positions and diameters of 197 Earth-crossing asteroids, plotted in (a, e) and (a, i) space. Any asteroid larger than 3 km is plotted with a large open circle. Any asteroid smaller than 200 m is plotted with a small open circle. The remaining asteroids are plotted with open circles linearly scaled between these limits. Asteroids crossing Earth's orbit lie between the $q = 1$ AU and $Q = 1$ AU lines, while asteroids crossing the orbits of the other planets lie between other (q, Q) lines. Few large asteroids are found at low e, though many small asteroids are located there. Small asteroids are also found at low i, though this may be the result of observational selection effects. Note that these trends match our expectations for an asteroid population modified by tidal forces (i.e. tidal disruption is likely when encounter velocities are low; compare this region with the low velocity region shown in Fig. 6)

relative to expectations based on the number of large ECAs seen elsewhere (Rabinowitz *et al.*, 1993; Rabinowitz, 1994). If real, few plausible sources other than tidal forces exist to produce this localized population (Bottke *et al.*, 1996c). The observational biases in the region, however, are difficult to calculate (for more detail, see Jedicke (1996)). More observational data is needed to verify Rabinowitz's claim.

7. Conclusions

We briefly summarize our results from this paper:

- Rubble-pile asteroids, after experiencing a close approach with Earth, frequently undergo tidal disruption, which can produce significant numbers of Tunguska-sized bodies.
- These disruptions are common where encounter velocities with Earth are low, corresponding to low values of e and i. These disruptions may explain the excess population reported by Spacewatch (Rabinowitz *et al.*, 1993; Rabinowitz, 1994).
- Our calculations show that an average mass production rate (upper limit) of 0.4 Tunguska-sized (50 m) objects per year is possible, and that this rate may be comparable to the ECA resupply rate of similarly sized bodies from the main belt.
- The size and orbital distributions of the known ECAs are consistent with the results of tidal disruption, which should be considered a positive argument that tidal forces play a prominent role in ECA evolution.

Acknowledgements. We thank the program committee and staff of Tunguska '96 (Bologna, Italy) for putting on such a well-run, interesting, and provocative conference. In particular, we thank Paolo Farinella, whose help was instrumental in getting us to participate at this meeting. Comments by referees Alan Harris, Paolo Farinella, and an anonymous reviewer have also been very valuable in producing this manuscript. This research was supported by William Bottke's Texaco Prize Fellowship at Caltech, Derek Richardson's Natural Sciences and Engineering Research Council (Canada) Fellowship, and Stanley Love's O. K. Earl Prize Fellowship at Caltech. This paper is Contribution 5752 of the Division of Geological and Planetary Sciences at the California Institute of Technology.

References

Aggarwal, H. R. and Oberbeck, V. R. (1974) Roche limit of a solid body. *Astrophys. J.* **191,** 577–588.

Asphaug, E. and Benz, W. (1994) Density of comet Shoemaker–Levy 9 deduced by modelling breakup of the parent "rubble pile". *Nature* **370,** 120–124.

Asphaug, E. and Benz, W. (1996) Size, density, and structure of comet Shoemaker–Levy-9 inferred from the physics of tidal breakup. *Icarus* **121,** 225–248.

Asphaug, E. and Melosh, H. J. (1993) The Stickney impact of Phobos—a dynamic-model. *Icarus* **101,** 144–164.

Belton, M. J. S. (1995) Bulk density of asteroid 243-Ida from the orbit of its satellite Dactyl. *Nature* **374,** 785–788.

Benz, W. and Hills, J. G. (1987) Three-dimensional hydrodynamical simulations of stellar collisions I. Equal-mass main-sequence stars. *Astrophys. J.* **323,** 614–628.

Benz, W., Hills, J. G. and Thielemann, F.-K. (1989) Three-dimensional hydrodynamical simulations of stellar collisions II. White dwarfs. *Astrophys. J.* **342,** 986–998.

Boss, A. P. (1994) Tidal disruption of periodic comet Shoemaker–Levy-9 and a constraint on its mean density. *Icarus* **107,** 422–426.

Boss, A. P., Cameron, A. G. W. and Benz, W. (1991) Tidal disruption of inviscid planetesimals. *Icarus* **92,** 165–178.

Bottke, W. F. and Melosh, H. J. (1996) The formation of asteroid satellites and doublet craters by planetary tidal forces. *Nature* **381,** 51–53

Bottke, W. F. and Melosh, H. J. (1996b) The formation of binary asteroids and doublet craters. *Icarus* **124,** 372–391.

Bottke, W. F., Nolan, M. C., Melosh, H. J., Vickery, A. M. and Greenberg, R. (1996) Origin of the Spacewatch small Earth-approaching asteroids. *Icarus* **122,** 406–427.

Bottke, W. F., Nolan, M. C. and Greenberg, R. (1994) Velocity distributions among colliding asteroids. *Icarus* **107,** 255–268.

Bottke, W. F., Nolan, M. C., Greenberg, R. and Kolvoord, R. A. (1994) Collisional lifetimes and impact statistics of near-Earth asteroids. In *Hazards Due to Comets and Asteroids*, eds T. Gehrels and M. S. Matthews, pp. 337–357. University of Arizona, Tucson.

Bottke, W. F., Richardson, D. C. and Love, S. G. (1997) Can tidal disruption of asteroids make crater chains on the Earth and Moon? *Icarus* **126,** 470–474.

Chandrasekhar, S. (1969) *Ellipsoidal Figures of Equilibrium.* Yale University Press, New Haven, Connecticut.

Dobrovolskis, A. R. (1982) Internal stresses in Phobos and other triaxial bodies. *Icarus* **52,** 136–148.

Dobrovolskis, A. R. (1990) Tidal disruption of solid bodies. *Icarus* **88,** 24–38.

Farinella, P., Froeschlé, Ch., Froeschlé, Cl., Gonczi, R., Hahn, G., Morbidelli, A. and Valsecchi, G. B. (1994) Asteroids falling into the Sun. *Nature* **371,** 314–317.

Froeschlé, Ch., Hahn, G., Gonczi, R., Morbidelli, A. and Farinella, P. (1995) Secular resonances and the dynamics of Mars-crossing and near-Earth asteroids. *Icarus* **117,** 45–61.

Greenberg, R., Nolan, M. C., Bottke, W. F., Kolvoord, R. A. and Veverka, J. (1994) Collisional history of Gaspra. *Icarus* **107,** 84–97.

Greenberg, R., Bottke, W. F., Nolan, M. C., Geissler, P., Petit, J. M., Durda, D. D., Asphaug, E. and Head, J. (1996) Collisional and dynamical history of Ida. *Icarus* **120,** 106–118

Grieve, R. A. F. and Shoemaker, E. M. (1994) The record of past impacts on Earth. In *Hazards Due to Comets and Asteroids*, eds T. Gehrels and M. S. Matthews, pp. 417–462. University of Arizona, Tucson.

Harris, A. W. (1996) The rotation rates of very small asteroids: evidence for "rubble-pile" structure. *Lunar Planet. Sci.* **XXVII,** 493–494.

Hills, J. G. (1994) Tsunami generated by small asteroid impacts. In *Hazards Due to Comets and Asteroids*, eds T. Gehrels and M. S. Matthews, pp. 779–789. University of Arizona, Tucson.

Hudson, R. S. and Ostro, S. J. (1995) Shape of asteroid 4769 Castalia (1989 PB) from inversion of radar images. *Science* **263,** 940–943.

Hudson, R. S. and Ostro, S. J. (1995) Shape and nonprincipal axis spin-state of asteroid-4179 Toutatis. *Science* **270,** 84–86.

Jedicke, R. (1996) Detection of near-Earth asteroids based on their rates of motion. *Astron. J.* **111,** 970–982.

Jeffreys, H. (1947) The relation of cohesion to Roche's limit. *Mon. Not. R. Astron. Soc.* **107,** 260–272.

Love, S. G. and Ahrens, T. J. (1996) Catastrophic impacts on gravity dominated asteroids. *Icarus* **124,** 141–155.

McFadden, L. A., Tholen, D. J. and Veeder, G. J. (1989) Physical properties of Aten, Apollo, and Amor asteroids. In *Asteroids II*, eds R. P. Binzel, T. Gehrels and M. S. Matthews, pp. 442–467. University of Arizona, Tucson.

Menichella, M., Paolicchi, P. and Farinella, P. (1996) The main-belt as a source of near-Earth asteroids. *Earth, Moon, and Planets* **72,** 133–149.

Michel, P., Froeschlé, Ch. and Farinella, P. (1996) Dynamical evolution of NEAs—close encounters, secular perturbations and resonances. *Earth, Moon, and Planets* **72,** 151–164.
Milani, A., Carpino, M., Hahn, G. and Nobili, A. M. (1989) Dynamics of planet-crossing asteroids—classes of orbital behavior—Project Spaceguard. *Icarus* **78,** 212–269.
Mizuno, H. and Boss, A. P. (1985) Tidal disruption of dissipative planetesimals. *Icarus* **63,** 109–133.
Morbidelli, A. and Moons, M. (1995) Numerical evidence on the chaotic nature of the 3/1 mean motion commensurability. *Icarus* **115,** 60–65.
Morrison, D. (ed.) (1992) *The Spaceguard Survey. Report of the NASA Near-Earth Object Detection Workshop.* NASA, Washington, DC.
Öpik, E. J. (1950) Roche's limit: rings of Saturn. *Irish Astr. J.* **1,** 25–26.
Öpik, E. J. (1966) Sun-grazing comets and tidal disruption. *Irish Astr. J.* **7,** 141–161.
Ostro, S. J. (1993) Planetary radar astronomy. *Rev. Mod. Phys.* **65,** 1235–1279.
Ostro, S. J. (1995) Extreme elongation of asteroid 1620-Geographos from radar images. *Nature* **375,** 474–477.
Ostro, S. J. (1995) Radar images of asteroid-4179 Toutatis. *Science* **270,** 80–83.
Ostro, S. J. (1996) Radar observations of asteroid 1620-Geographos. *Icarus* **121,** 46–66.
Passey, Q. and Melosh, H. J. (1980) The effects of atmospheric break-up on crater field formation. *Icarus* **42,** 211–233.
Rabinowitz, D. L. (1994) The size and shape of the near-earth asteroid belt. *Icarus* **111,** 364–377.
Rabinowitz, D. L. (1993) Evidence for a near-earth asteroid belt. *Nature* **363,** 704–706.
Richardson, D. C. (1993) A new tree code method for simulations of planetesimal dynamics. *Mon. Not. R. Astron. Soc.* **261,** 396–414.
Richardson, D. C. (1994) Tree code simulations of planetary rings. *Mon. Not. R. Astron. Soc.* **269,** 493–511.
Richardson, D. C. (1995) A self-consistent numerical treatment of fractal aggregate dynamics. *Icarus* **115,** 320–335.
Richardson, D. C., Bottke Jr, W. F. and Love, S. G. (1997) (in preparation).
Sekiguchi, N. (1970) On the fission of a solid body under influence of tidal force. *Moon* **1,** 429–439.
Solem, J. C. and Hills, J. G. (1996) Shaping of Earth-crossing asteroids by tidal forces. *Astron. J.* **111,** 1382–1387.
Sridhar, S. and Tremaine, S. (1992) Tidal disruption of viscous bodies. *Icarus* **95,** 86–99.
Thomas, P., Veverka, J., Bell, J., Lunine, J. and Cruikshank, D. (1992) Satellites of Mars: geologic History. In *Mars*, eds H. H. Kieffer, B. M. Jakosky, C. W. Snyder and M. S. Matthews, pp. 1257–1282. University of Arizona, Tucson.
Wasson, J. T. (1974) *Meteorites.* Springer, New York.
Weissman, P. R. (1982) Terrestrial impact rates for long- and short-period comets. *GSA Special Paper* **190,** 15–24.
Wisdom, J. (1983) Chaotic behavior and the origin of the 3/1 resonance. *Icarus* **56,** 51–74.